Surface Fractality of Wood Charcoals through Small-Angle X-Ray Scattering

A. Venkatraman, A. A. Boateng, L. T. Fan, and W. P. Walawender
Dept. of Chemical Engineering, Kansas State University, Manhattan, KS 66506

Geometrical properties of the pore-solid interfaces of devolatilized charcoals from the pyrolysis of fuel woods in a bench-scale fluidized-bed reactor were investigated through small-angle X-ray scattering. Specifically, surface morphological features of the interfaces were characterized by a single parameter indicative of the degree of surface roughness, that is, the surface fractal dimension, d_{SF}, at various retention times. The surface fractal dimensions of the original wood samples prior to devolatilization were approximately identical for all species within the range between 2.00 and 2.15, over a length scale from 55 to 600 Å, and those for the respective charcoals from these wood samples were influenced to different degrees by the retention time, τ, in the reactor. The d_{SF}'s of the mesopores of charcoals of all the species attained maxima at a value of τ equal to 35 s and decreased subsequently with an increase in τ. The analysis of this unexpected trend was facilitated by the values of the mean radii of gyration of the pores, estimated through the Guinier plots. The results imply that when the retention time of the charcoals in the reactor is prolonged, the mechanism of pore enlargement and smoothening of the interfaces can play a dominant role in altering the surface morphology and thereby influence significantly the kinetics of chemical reactions in heterogeneous porous systems.

Introduction

A quantitative measure of surface roughness based on the concept of the surface fractal dimension, d_{SF}, is increasingly becoming a popular tool in characterizing the morphology of particulate materials (Pfeifer et al., 1989). There has been a growing recognition that surface fractals comprise the largest and most diverse type of fractal objects found in nature (Avnir and Farin, 1992). The d_{SF}, a relative measure of how well a surface fills three-dimensional space, takes on values between 2.0 and 3.0, depending on the degree of irregularity. Smooth surfaces are associated with a value of 2.0, while surfaces that are extremely convoluted, that is, volume-filling, have values approaching 3.0 (Pfeifer and Avnir, 1983; Feder, 1988; Fan et al., 1991).

The intrinsic nature of surface fractality in porous systems has been revealed repeatedly through various surface-probing methods such as those based on adsorption, electronic energy transfer, and small-angle X-ray and neutron scattering (Avnir et al., 1983, 1984; Bale and Schmidt, 1984; Hall and Williams, 1985; Fripiat et al., 1986; Pines and Huppert, 1987; Pines et al., 1988). The significance of irregularities on the surface of solid reactants is obvious; however, the role played by such irregularities cannot be readily understood through the traditional geometrical considerations (Pfeifer and Avnir, 1983). Novel tools are needed, therefore, to elucidate the interdependence between the characteristics of the surface and its chemical reactivity in processes such as char gasification and catalysis. Traditionally, the effect of pore structure in heterogeneous reactions is accounted for by an effectiveness factor, defined as the ratio of the actual rate of reaction within a pore to the rate of reaction in the absence of pore resistance (Satterfield and Sherwood, 1963; Satterfield, 1970; Gates, 1992). The combination of the effectiveness factor and the Thiele modulus often categorizes the importance of the pore resistance relative to that of the chemical reaction in porous media. Alternatively, the random-pore model can serve to relate the changes of reaction surface area, a measurable quantity, with a combination of chemical and

Correspondence concerning this article should be addressed to L. T. Fan.
Present address of A. A. Boateng: Solite Corp., P.O. Box 27211, Richmond, VA 23261.

pore-size effects (Bhatia and Perlmutter, 1980, 1981; Gavalas, 1980; Su and Perlmutter, 1985). Nevertheless, a comprehensive and recondite understanding of phenomena such as gas–solid reactions in porous media cannot be gained without taking into account the intrinsic fractal nature of such media.

The fractal nature of porous structures can be perceived in two ways. The first is a self-similar branching pore-tree in which every pore bifurcates into several smaller ones, thereby resulting in a fractal pore-size distribution (Pape et al., 1984; Sheintuch and Brandon, 1989), and the second is in terms of irregularities on the surfaces of the pores that scale with the yardstick of measurement, thus giving rise to interfacial fractal dimensions (Adler, 1989, 1992; Fan et al., 1991; Dullien, 1992). Both approaches have been employed to investigate the influence of d_{SF} on the rates of heterogeneous reaction and diffusion through porous media (Sheintuch and Brandon, 1989; Gutfraind et al., 1991; Gutfraind and Sheintuch, 1992; Seri-Levy and Avnir, 1991; Coppens and Froment, 1995a,b). The d_{SF} is, therefore, an important parameter in the mathematical modeling of chemical reaction rates; thus, various techniques have been sought recently to obtain a reliable value for d_{SF}. These techniques mainly involve different probing methods, of which the most popular is physisorption, modeled by the BET equation, whereby the surface is probed successively with adsorbates of similar shapes but different molecular sizes such as argon, krypton, xenon, or the members of the homologous series of hydrocarbons. The ensuing power-law relationship between the measured value of the surface area based on monolayer coverage, and the size of the probing molecule is typical for rugged surfaces. A porous surface is said to be fractal if the pore–solid interface is scale invariant; hence, the determination of d_{SF} requires yardsticks having the capability of probing all the interfacial irregularities or bumps over a given size range. In the light of this, Rojanski et al. (1986) have demonstrated that the values of d_{SF} for a mesoporous silica gel, obtained from three different probing methods, are consistent. These methods are: (1) adsorption with several adsorbates of varied sizes as well as with assorted-size fractions of the same adsorbent; (2) small-angle X-ray scattering (SAXS); and (3) dipolar energy transfer.

The present work involves the characterization of the pore-solid interfaces of the charcoals obtained from the pyrolysis of various hardwood species in a bench-scale fluidized-bed reactor at 1,073 K. The hardwoods comprised high, medium, and low specific gravity woods of Black Locust, Siberian Elm, and Silver Maple, respectively. Specifically, the d_{SF} of the interfaces of the mesopores of the charcoals have been determined through SAXS at various τ's; the mean radii of gyration R_g of the mesopores and micropores have also been estimated from the scattering data obtained. Furthermore, the macropores of the charcoals have been examined by secondary electron microscopy (SEM) at a resolution of a few microns. Hence, the current work investigates the evolution of the surface morphological features of the interfaces of the hardwoods with progress in τ by employing two different length scales of observation.

Theoretical Studies

X-rays are scattered primarily by electrons of an irradiated material. The distribution of electrons throughout the material is not homogeneous, and there exist fluctuations in electronic density (number of electrons/unit volume) at different regions of the sample. When the dimensions of these spatial inhomogeneities are similar to the wavelength, λ, of the incident X-ray beam, then most of the scattering is observed at angles greater than 10°, as in conventional X-ray diffraction patterns. On the other hand, if the heterogeneities in the electronic density extend over distances in the interval between approximately 5 and 4,000 Å, then the intensity of the scattered X rays would be appreciable at *small* angles, that is, a few degrees or less (Guinier et al., p. 3, 1955; Glatter and Kratky, 1982). Thus, the small-angle X-ray scattering technique can provide information on structures appreciably larger than the normal interatomic distances encountered in dense materials. As a result, it has been widely employed to investigate the structures of various disordered materials on length scales varying from 5 to 4,000 Å (Schmidt et al., 1995). A schematic of a typical SAXS system is shown in Figure 1. Conventionally, small angles imply that the values of the scattering angle, 2θ, are no greater than 6°.

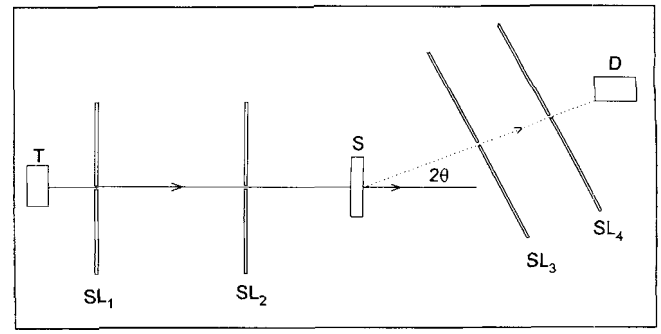

Figure 1. SAXS system.

T denotes the X-ray tube; SL_1, SL_2, SL_3, and SL_4, the collimating slits; *S*, the sample holder; and *D*, the detector.

The intensity of the scattered X-rays, $I(q)$, from a disordered material with a random distribution of pores, within the solid phase of the porous media, is a function of the scattering wave vector, q, whose magnitude is expressed as

$$|q| = 4\pi(\Theta)/\lambda. \tag{1}$$

The general theoretical expression for $I(q)$ can often be reduced to various forms depending on the value of the product, qd (Guinier et al., pp. 2, 26, 1955; Schmidt, 1994), where d is a length characterizing the "size" of a structure producing the scattering, for example, the average pore size or the average diameter. Note that most of the structural information on the sample obtainable from the scattering data is contained in the measurements at the values of q satisfying the condition (Kalliat et al., 1981)

$$0.1 < qd < 10. \tag{2}$$

Furthermore, a general property of the scattering theory indicates the existence of an inverse relationship between q and the length scale on which structural information is obtainable (Schmidt et al., 1989). Consequently, three distinct regimes can be identified in most SAXS data sets, with each regime being associated with a characteristic range of values

of values of qd. Suppose that qd is much smaller than one, signifying the first regime; then, $I(q)$ will be constant, that is, essentially be independent of q. Hence, in this regime, information on the structure of the scatterers cannot be obtained (Schmidt, 1994). On the other hand, when the condition of being in the second regime, that is, qd being appreciably greater than 1.0, is satisfied, then $I(q)$ can be approximated by the Porod equation, Eq. 5, in terms of a power-law function of q. The third regime can be identified with the scattering from systems of isotropic, randomly oriented, independent scatterers, wherein $I(q)$ can be approximated by the Guinier equation

$$I(q) = I(0)\exp\left[-(qR_g)^2/3\right] \tag{3}$$

for values of qd not appreciably greater than 1.0 (Guinier et al., p. 24, 1995). The mean radii of gyration of the scatterers, R_g, can be evaluated in this regime from the slope of a plot of the natural logarithm of $I(q)$ vs. q^2. An order-of-magnitude estimate of d is obtainable from R_g if the shape and charge distribution of the scatterers are known; usually, $2R_g < d < 3.5\ R_g$ (Schmidt et al., 1995). Specifically, if the system of scatterers can be assumed to be composed of identical, spherical pores of radius r_0, then the relation, $r_0 = 1.3\ R_g$, can be applied to obtain r_0 (Guinier et al., p. 26, 1995).

For a porous material with the solid fraction, c, the total volume, V, and the uniform (constant) electronic density of the solid phase, δ, the scattered intensity, $I(q)$, can be expressed as (Guinier et al., p. 78, 1955; Bale and Schmidt, 1984; Wong and Bray, 1988a)

$$I(q) = 4\pi I_e \delta^2 c(1-c)V\int_0^\infty r^2 g(r)[\sin(qr)/(qr)]\,dr. \tag{4}$$

The rationale for assuming δ be a constant is based on the fact that small-angle X-ray scattering cannot resolve atomic-scale structures (Guinier et al., p. 3, 1995). For a porous medium with a total interfacial area of A between the two phases comprising the pore and solid for values of qd far greater than 1.0, the scattered intensity has been shown to be proportional to q^{-4} or Θ^{-4} (Porod, 1951; Guinier et al., pp. 17, 80, 1955) or,

$$I(q) = 2\pi I_e \delta^2 A q^{-4}. \tag{5}$$

The Porod relationship, Eq. 5, is valid only when the boundaries of the pores can be considered as smooth, that is, free from irregularities. When the surfaces of the pores are fractal (Mandelbrot, 1982), the scattered intensity can be modified through the correlation function, $g(r)$ (Glatter and Kratky, 1982), to take cognizance of the surface irregularities. One of the characteristic features of a fractal surface is that the total volume, V_b, of spheres or molecules with a diameter of r, required to cover the surface completely, is given by (Avnir et al., 1983; Pfeifer et al., 1983; Fan et al., 1991)

$$V_b = N_0 r^{(3-d_{SF})}. \tag{6}$$

Bale and Schmidt (1984) have demonstrated that the correlation function, $g(r)$, for a fractal surface takes the form

$$g(r) = 1 - [N_0 r^{(3-d_{SF})}]/[4c(1-c)V], \tag{7}$$

which, on insertion into Eq. 4, yields the following relationship between the scattered intensity and d_{SF} for the values of qd far greater than 1.0.

$$I(q) = \pi I_e \delta^2 N_0 \Gamma(5-d_{SF})\sin[\pi(d_{SF}-1)/2]/q^{(6-d_{SF})}. \tag{8}$$

Consequently, when d_{SF} equals 2.0, Eq. 8 reduces to Eq. 5 (the classical Porod equation), and N_0, the characteristic constant of the fractal surface, reduces to A; in fact, N_0 can be considered to be the fractal generalization of A of a smooth surface (Schmidt et al., 1989). Note that the prefactor of Eq. 8 can be replaced by a constant, I_0, to yield the following power-law expression for $I(q)$, which is applicable only for the values of qd far greater than 1.0 (Schmidt, 1991; Schmidt et al., 1989)

$$I(q) = I_0 q^{-\alpha}. \tag{9}$$

The value of α is bounded between 3.0 and 4.0, corresponding to values of d_{SF} approaching 3.0 and equal to 2.0, respectively.

When d_{SF} approaches 3.0, however, $I(q)$ vanishes according to Eq. 8; this apparent dilemma has been discussed at length by Rojanski et al. (1986), Pfeifer and Schmidt (1988), Wong and Bray (1988b), and Schmidt (1989). Rojanski et al. (1986) have proposed a higher order approximation for $I(q)$ in the limit as d_{SF} approaches 3.0. By including an additional term proportional to q^{-4}, $I(q)$ in Eq. 8 does not vanish, but has a q^{-4} dependence as d_{SF} approaches 3.0; therefore, the exponent, α, in Eq. 9 has a value of 4.0 for both d_{SF} equal to 2.0 and d_{SF} equal to 3.0. A definitive expression for the scattered intensity in the limit as d_{SF} approaches 3.0 has not yet been reported. The general consensus is that if a q^{-4} power-law dependence for $I(q)$ is determined from the scattering data, then it does not always imply that the value of d_{SF} equals 3.0, unless the latter is validated by other independent techniques such as electronic energy and gas adsorption (Schmidt, 1989).

Experimental

The d_{SF} of charcoals obtained from the pyrolysis of various wood species have been determined from measurements of the intensities of the X-rays scattered at various small angles; SEM and image analysis supplemented the interpretation of the results from SAXS. The length scale of observation for SEM was of the order of a few microns, while that for SAXS ranged from approximately 8 to 600 Å.

Sample preparation

The samples of charcoals were generated by devolatilizing three species of hardwoods, Black Locust (*Robinia pseudoacacia*), Siberian Elm (*Ulmus pumila*), and Silver Maple (*Alcer saccharinum*), in a bench-scale fluidized-bed reactor operating at 1,073 K. The reactor was constructed from a 5.08-cm

(2-in.) schedule 40 pipe of Inconel 600 alloy and was heated externally by two pairs of semicylindrical, electrical-resistance heaters (Boateng et al., 1991; Boateng et al., 1992). The wood samples were in the form of chips, each with a thickness between 4 and 10 mm; these samples were produced by chipping and drying, and had been stored for over 8 years. The final moisture content ranged between 7.2 and 8.2%. Two samples of charcoals from each species, discharged from the reactor at retention times of 35 and 60 s, and deemed terminal, that is, completely devolatilized, were acid-washed to reduce their content of mineral matter to insignificant amounts. The samples were prepared for subsequent SAXS and SEM/image analyses.

SAXS

Each sample of the terminal charcoal was ground and seived to a size fraction to ensure uniformity in the packing of the sample cell of a fully automated X-ray diffractometer system (Scintag XDS 2000). The X-ray tube of the system featured a copper target and a stationary anode, and was operated at 40 kV and 25 mA. A Beeman four-slit collimation system (Anderegg et al., 1955; Beeman, 1967) was employed in conjunction with the apparatus, as shown in Figure 1. The length and width of the collimating slits were 10 mm and 0.25 mm, respectively, and the spacing between successive slits was 50 cm. The X-rays scattered by the sample at small angles were intercepted by a liquid-nitrogen-cooled germanium solid-state detector. Monochromatization of the incident beam and removal of continuum X-rays were performed by a combination of a nickel filter and a pulse-height analyzer (Ortec 590A AMP/SCA) to ensure that electrical pulses corresponding to only the Cu K-α emission spectrum at a wavelength of 1.54 Å reached the ratemeter (Scintag Ratemeter) of the system.

The intensities of the scattered beam were recorded over a range of scattering angles varying from approximately 1.3×10^{-3} to 1.1×10^{-1} radians; an automated electronic programmer facilitated the selection of the desired angles. Measurements of the scattered intensities were repeated for reproducibility, time averaged to account for the day-to-day fluctuations in the intensity of the incident X-ray beam, and corrected for the background contribution of the sample cell and molecules of air in the system. In addition, the system was calibrated to account for the dead-time losses in the solid-state detector. Furthermore, corrections to account for the reduction of intensity resulting from photoelectric absorption by the samples was accomplished by dividing the measured scattered intensity for a sample by the experimentally determined value of the corresponding transmission, T.

The data on the measured intensities have also been corrected for the effects of the finite length of the collimating slits through a software routine that performs deconvolution. The computer algorithm for the collimation corrections is based on the procedure developed by Lin et al. (1974), wherein the weighting function for the intensity distribution along the length of the slits (Hendricks and Schmidt, 1967) is approximated by a Gaussian. Furthermore, the routine resorts to a standard propagation-of-error technique to estimate the statistical uncertainties in the corrected scattering data. It has been assumed that these uncertainties are due only to the random statistical errors in the measured intensities. Moreover, the random statistical error associated with each value of the measured intensity in the small-angle range has been considered to be proportional to the square root of that measured intensity, that is, the number of counts recorded (Lin et al., 1974), since the counting times were identical in all the measurements.

Corrections to account for effects of the width of the slits were deemed unnecessary. The width of the slits was considerably smaller than their length, and it was assumed that the former had a negligible effect on the scattering pattern.

Corrections to the data on the measured intensities have also been carried out for the effects of possible differences in the *volumes* of the various irradiated samples. Although the arrangement of the collimating system was identical for all samples so that the irradiated cross-sectional areas were the same, variations can arise in the thickness of the samples in a direction parallel to the incident X-ray beam. Hence, to account for these effects, the measured intensities have been multiplied by the factor $\rho\mu_m/\ln(1/T)$ (Kalliat et al., 1984; also see the Appendix). Note that the samples of charcoal were assumed to be composed entirely of amorphous carbon, with a μ_m value of 4.5 cm^2/g (Compton and Allison, 1935); the values of μ_m for the various species of wood, on the other hand, were estimated from their respective elemental compositions. In addition, the specific gravities of the different samples were measured; the values for the species of wood ranged between 0.3 and 0.5 g/cm^3, while those for the charcoals ranged from 0.6 to 0.9 g/cm^3.

The effects of multiple scattering were negligible for all the samples, since essentially equivalent scattering curves were obtained for varying thickness of each sample.

Data acquisition, control and analysis as well as the complete automation of the diffractometer system were done by a minicomputer (MicroVax 2000, VMS operating system).

SEM/image analysis

The microstructures of the pores at various sites on each charcoal were observed and recorded on Polaroid films with the aid of a SEM apparatus (ETEC Autoscan) at a resolution of a few microns. The network of the macropores was examined by analyzing the photomicrographs with an image analysis system (Buehler 80-1000-160 Omnimet Image Analysis System, replete with a high-resolution Vidicon Precision Scanner, Analysis Module, and a Video Monitor). Thus, it was possible to determine the mean number of pores per unit area, that is, mean pore number density, as well as the mean pore size and average area of the macropores for each sample of wood charcoal.

Results and Discussion

Significant results are presented and analyzed here.

Terminally devolatilized charcoals

The mean value of the terminal charcoal yield for each sample is in Table 1. It is obvious from this table that the

Table 1. Terminal Charcoal Yields for Wood Samples

Wood Species	Moisture Content	Terminal Charcoal Yield* Mean	Std. Dev.
Siberian Elm *(Ulmus speciosa)*	7.0%	14.6%	±0.4%
Black Locust *(Robina pseudoacacia)*	7.2%	13.2%	±0.3%
Silver Maple *(Acer saccharinum)*	7.7%	10.9%	±0.3%

*Oven-dry basis.

species with the maximum and minimum contents of volatile matter are Silver Maple and Siberian Elm, respectively.

SEM/image analysis

The typical SEM photomicrographs of the terminal charcoals, retrieved after 35 and 60 s of devolatilization, for the three species are displayed in Figures 2 to 4. The dark and light regions represent the pores and solid matter, respectively, and the magnification and length scale are indicated at the bottom of each figure. The structures of the pores observable are those for the macropores of a few microns in diameter; their nature and shapes are also clearly visible. The pore dimensions and number counts for each species of charcoal have been calculated from the exposed (dark) areas with the image analyzer, and the mean computed from the values thus obtained from four photomicrographs taken at various sites. The results, summarized in Table 2, show that the mean pore number density for both Siberian Elm and Silver Maple decreased when τ was increased from 35 s to 60 s; this is consistent with the concomitant increase in the average diameters of the pores at the length scale of observation. For Black Locust, the increase in the mean pore number density with the attendant inconsistent decrease in the average size of the macropores is indicative of fragmentation rather than pore growth.

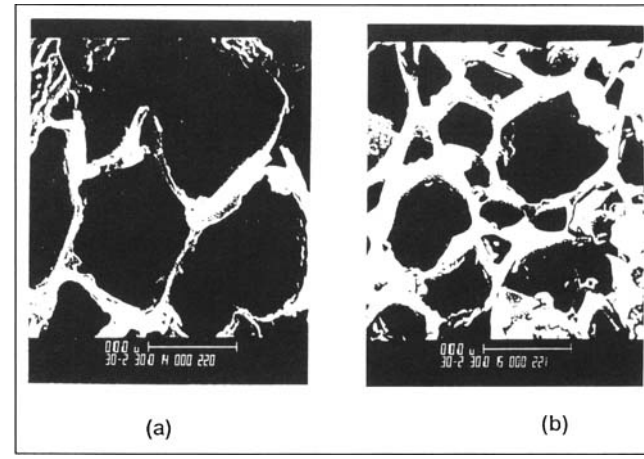

Figure 3. SEM on charcoals of Black Locust produced at various retention times: (a) 35 s; (b) 60 s.

SAXS data

The intensities of the scattered X-rays measured experimentally at small angles or, equivalently, small values of the scattering wave vector, q, have been corrected for the effects of the background scattering, slit-length collimation, photoelectric absorption, and the variations in the volumes of the irradiated samples for the three species investigated. The corrected scattering curves for the samples of Siberian Elm, Black Locust, and Silver Maple, are depicted in Figures 5, 6 and 7, respectively. Note that the intensities are expressed in dimensionless units, that is, relative to an arbitrary system of measurement in terms of counts per second. Thus, all the plots involve the relative rather than the absolute intensity, since the latter requires determining the cross-sectional areas of the scattering medium (Setek et al., 1984), a task not performed in the present work. The scales for the relative intensities are identical in all the plots. The intensities scattered from different samples can be compared directly from these plots since the curves correspond to scattering from samples with the same mass per unit area, M/A_0, of irradiation.

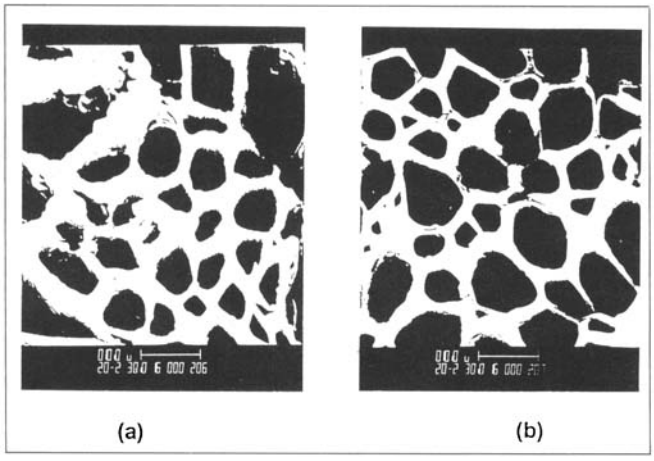

Figure 2. SEM on charcoals of Siberian Elm produced at various retention times: (a) 35 s; (b) 60 s.

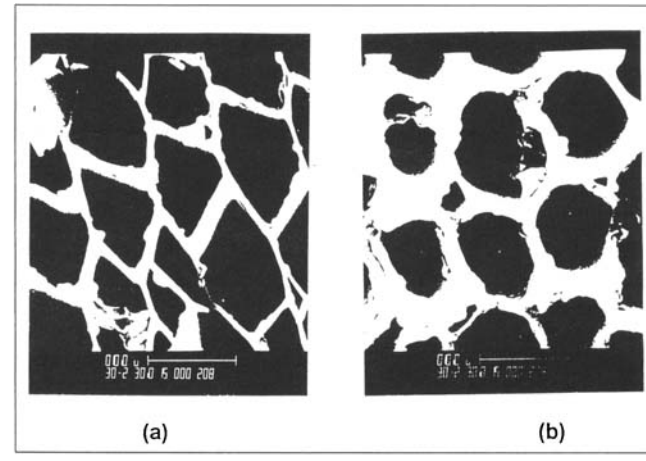

Figure 4. SEM on charcoals of Silver Maple produced at various retention times: (a) 35 s; (b) 60 s.

Table 2. Macropore Analysis of Various Charcoals with SEM and Image Analyzer

Wood Species	Retention Time s	Pore No. Density mm^{-2}	Avg. Pore Area $\times 10^5$ mm^2	Avg. Pore Dia. $\times 10^3$ mm
Siberian Elm	35	12,500	3.10	6.3
	60	8,700	5.43	8.3
Black Locust	35	4,890	18.53	15.3
	60	13,600	5.25	8.1
Silver Maple	35	5,430	7.78	10.1
	60	3,950	12.10	12.4

Figures 5 to 7 indicate that the corrected scattering curves for all the samples of wood are similar and are very distinct from those for the charcoals. For the sample of each species of wood, a power-law regime is discernable over an interval of values of q ranging from approximately 5.3×10^{-3} $Å^{-1}$ to 5.7×10^{-2} $Å^{-1}$. In addition, a characteristic "bump" or convex region is observable for values of q ranging from approximately 7.0×10^{-2} $Å^{-1}$ to 1.8×10^{-1} $Å^{-1}$. This bump can be attributed to the scattering from the crystalline cellulose in the unpyrolyzed samples of wood (Cutter et al., 1980). A detailed interpretation will need to consider the scattering from both the cellulose and pores in this region, a task beyond the scope of the present work.

On the other hand, each corrected scattering curve for the charcoals displays two power-law regions connected by a distinct "shoulder" at a value of q that is approximately 0.015 $Å^{-1}$ (Figures 5 to 7). Furthermore, in the outer part of the curve, the intensity is observed to decay much more slowly relative to the power-law regions. The prominent power-law region, that is, the one to the right of the shoulder, observable over an interval spanning approximately an order of magnitude in values of q, is attributable to the scattering from the mesopores, while the other—the one to the left of the shoulder that is relatively short and less significant—can be considered to be due to the macropores. The shoulder thus is indicative of the existence of two different length scales of inhomogeneities responsible for the observed scattering (Kalliat et al., 1981; Schmidt, 1994). Note that the slowly decaying outer part is ascribed to the scattering from the micropores (Bale et al., 1984). Hence, the porous structure of each sample of charcoal can be characterized by three different length scales corresponding to the macropores, mesopores, and micropores. Thus, the total intensity scattered can be considered to be the sum of the intensities from the three types of pores provided that they scatter independent of each other.

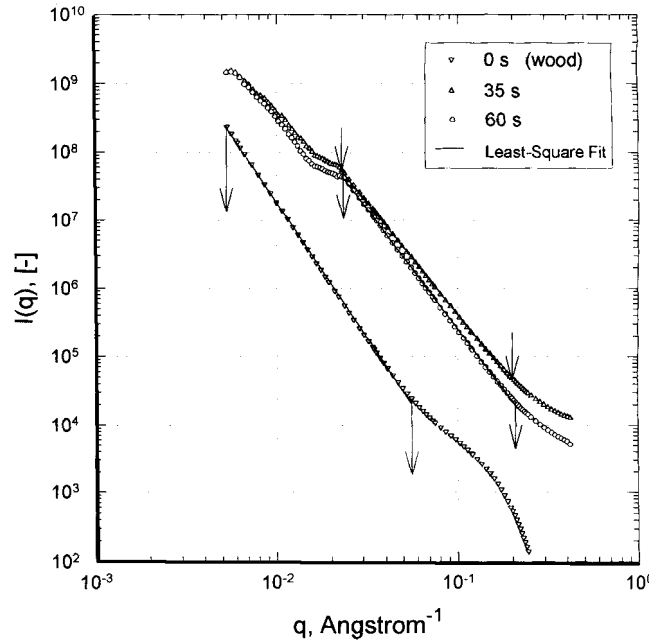

Figure 6. Relative scattered intensity vs. scattering wave vector for Black Locust.

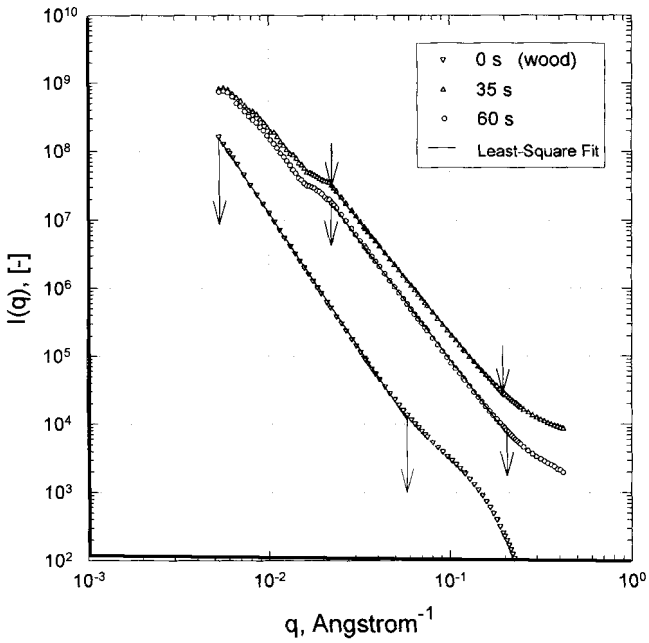

Figure 5. Relative scattered intensity vs. scattering wave vector for Siberian Elm.

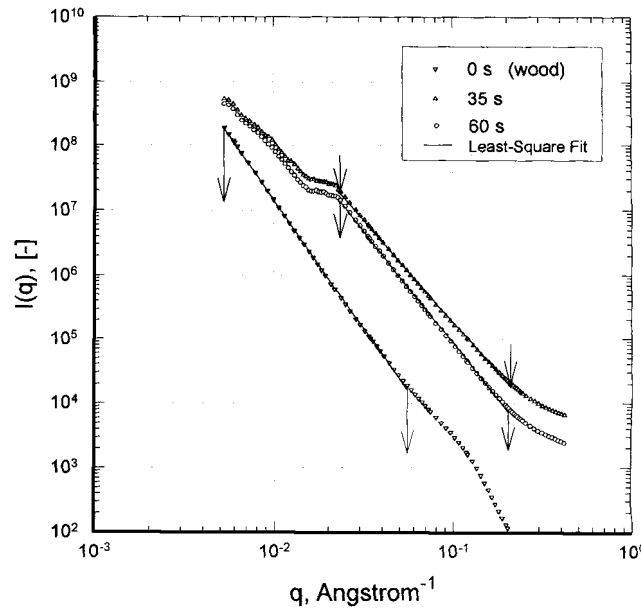

Figure 7. Relative scattered intensity vs. scattering wave vector for Silver Maple.

Surface fractal dimension from SAXS

The exponent, α, of Eq. 9 has been determined from the slope of the mesopore power-law regime of each logarithmic plot presented in Figures 5 through 7, by a weighted, first-order least-square fit of the data (Bevington, 1969; Margerison, 1969) over the range of q's shown. The fit in each plot assigned a weight to every data point of the corrected intensity that is inversely proportional to the square of the calculated statistical uncertainty in the value of the corrected intensity. The nonintegral values of α, bounded between 3.0 and 4.0, obtained for the terminal charcoals imply that their relative scattered intensities do not conform to the classical Porod law, Eq. 5, over the interval of approximately, 2.2×10^{-2} Å$^{-1} < q < 2.2\times 10^{-1}$ Å^{-1}. Instead, the interfaces of the mesopores of these samples can be considered to exhibit fractal properties within this range of q, or alternatively, the power-law distribution of the mesopores can be associated with a nonintegral dimension (Bale et al., 1984). Consequently, the d_{SF} for each sample has been determined from the corresponding α. The results are tabulated in Table 3 for all the samples; also displayed in the table are the uncertainties in the values of d_{SF} and the power-law intervals of q's. The uncertainties are attributable to the uncertainties associated with the slopes of the weighted least-square fits. Note that the power-law region for the macropores of each sample of charcoal has not been included in the analysis since it does not extend over a large enough interval of q to facilitate the computation of meaningful and reliable values of α. Furthermore, the length scale, ξ, associated with a given value of q can be estimated from the approximate Bragg relation, $\xi = \pi/q$ (Hohr et al., 1988); thus, it is evident from Table 3 that the interfaces of the mesopores of the charcoals are fractal over yardsticks ranging from approximately 15 to 150 Å.

As can be seen in Table 3, the values of d_{SF} for all three species of the wood samples prior to devolatilization do not exceed 2.1 ± 0.10, over an approximate interval, 5.3×10^{-3} Å$^{-1} < q < 5.7\times 10^{-2}$ Å^{-1}; this is an indication that the interfacial surfaces of both the macropores and mesopores are relatively smooth and that for all practical purposes, the samples can be regarded as nonfractal. Marked increases are expected in the values of d_{SF} for all the wood species on carbonization; a degradation and subsequent rearrangement of the carbon skeleton combined with the violent release of the volatile matter are likely to generate rough interfacial surfaces. The values of d_{SF} for the charcoals of Silver Maple, however, are higher than those for the charcoals of the other two species at both τ's of 35 and 60 s. The plausible influence of the content of volatile matter in each of the unpyrolyzed wood species on the d_{SF} of the corresponding terminal charcoal is expected, as inferred from Tables 1 and 3; the larger the amounts of volatiles released, the greater the degree of irregularity in the porous interfaces of the charcoals.

Table 3. Surface Fractal Dimensions, d_{SF}, of Various Charcoals and Unpyrolyzed Wood Species

Wood Species	Retention Time s	d_{SF}	$q_{minimum}\times 10^2$ Å^{-1}	$q_{maximum}\times 10^2$ Å^{-1}
Siberian Elm	0	2.02 ± 0.11	0.53	5.84
	35	2.69 ± 0.09	2.13	20.0
	60	2.50 ± 0.08	2.13	21.1
Black Locust	0	2.03 ± 0.08	0.53	5.45
	35	2.73 ± 0.11	2.12	20.1
	60	2.48 ± 0.10	2.21	21.3
Silver Maple	0	2.05 ± 0.11	0.53	5.55
	35	2.81 ± 0.10	2.18	21.1
	60	2.51 ± 0.08	2.17	21.0

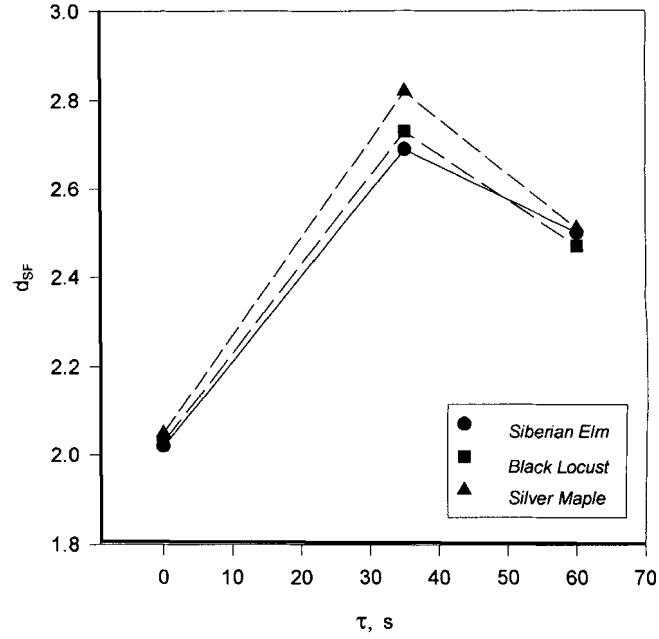

Figure 8. Variation of the surface fractal dimension with the retention time.

It is discernable from Table 3 that d_{SF} varies with τ for each species. This trend, highlighted in Figure 8, can be attributed to the increase in the mean size of the pores with an increase in the value of τ from 35 to 60 s. This rationale has been substantiated by the mean radii of gyration of the micropores and mesopores, estimated from the Guinier plots, as described in the succeeding subsection. A mechanism involving the smoothening of the interfaces of the pores with the progress in τ may account for the observed decrease in the values of d_{SF}. Note that the heating rates involved in the pyrolytic experiments were identical for all the samples, and therefore could not have been a contributing factor. This phenomenon, observed during the pyrolysis of a naturally occurring product, is yet to be investigated thoroughly; further studies are anticipated.

Mean radii of gyration

The mean radii of gyration R_g of the *micropores* of each sample of charcoal, whose scattering is evident in the outer portion of the curves shown in Figures 5 through 7, has been obtained by applying Eq. 3 to the Guinier plots presented in Figures 9 to 11. Also shown on each plot is a typical interval of q that satisfies the Guinier equation, Eq. 3. Note that this equation is valid only when the product, qR_g, is not appreciably greater than 1.0. Furthermore, the scattering system must be composed of randomly oriented, independent scatterers (Schmidt et al., 1995).

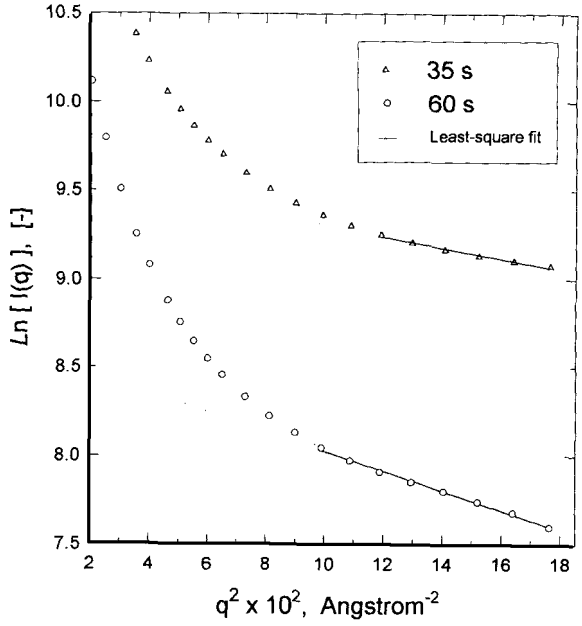

Figure 9. Guinier plot for estimating the mean radii of gyration of micropores of Siberian Elm at various retention times.

The value of R_g obtained for each of the terminal charcoals is tabulated in Table 4; the range of values of q over which the computations have been performed in each case, is also presented. It can be observed that R_g depends on the interval chosen for the calculation, in spite of the fact that only those values of q in the outer region of each plot have been included; see Figures 9 through 11. It is obvious that a number of linear least-square fits of the data in the outer region can be carried out over slightly differing ranges of q; however, each fit is associated with a different slope. Hence, the uncertainties in R_g indicated in Table 4 are basically attributable to the difficulties inherent with defining precisely both the location and the desired length of the interval of linearity. Only those fits that satisfied the empirical condition, $q_{\max} R_g$ *less than or equal to 1.7*, over a fairly *long* linear interval have been averaged to yield the mean value of R_g for each sample. This averaging process contributes substantially to the total uncertainty in R_g; in contrast, the uncertainty in the slope of the weighted least-square fit is relatively small and negligible.

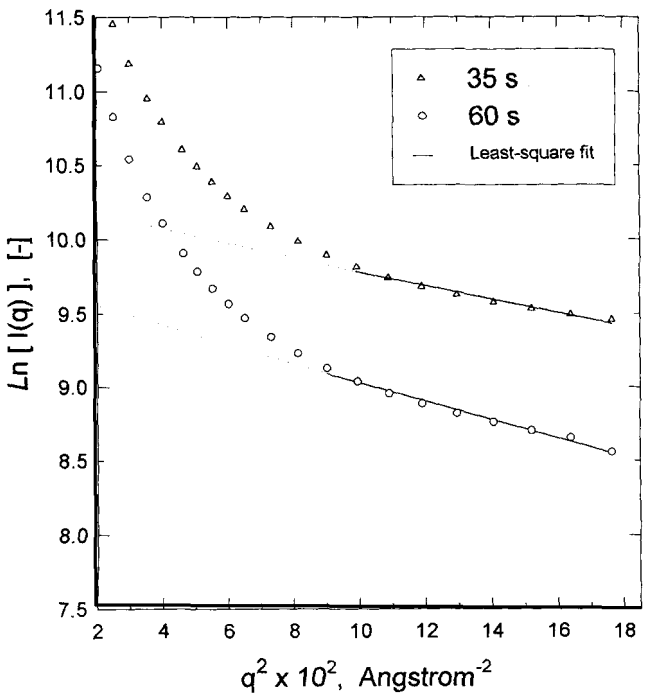

Figure 10. Guinier plot for estimating the mean radii of gyration of micropores of Black Locust, at various retention times.

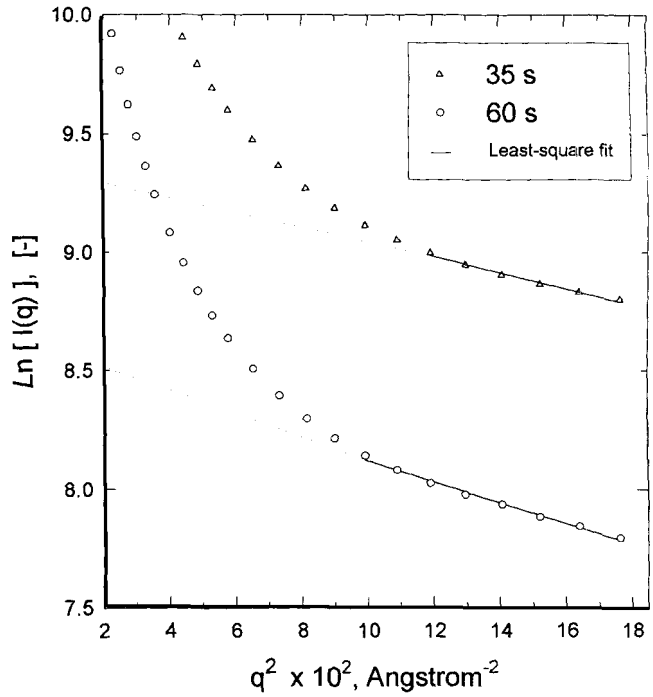

Figure 11. Guinier plot for estimating the mean radii of gyration of micropores of Silver Maple at various retention times.

The increase in the value of R_g of the micropores of each species of charcoal from the retention time of 35 s to that of 60 s, observable in Table 4, can be ascribed to a possible coalescence of the micropores. This rationale is based on the ratio of the intercept, $I(0)$, of each Guinier plot to the sixth

Table 4. Mean Radii of Gyration of Micropores of Various Wood Charcoals

Wood Species	Retention Time s	R_g Å	$q_{\text{minimum}} \times 10^2$ Å^{-1}	$q_{\text{maximum}} \times 10^2$ Å^{-1}
Siberian Elm	35	3.02±0.28	2.82	4.20
	60	4.07±0.33	2.97	4.20
Black Locust	35	3.68±0.30	2.44	4.20
	60	4.40±0.37	2.56	4.20
Silver Maple	35	3.20±0.30	2.69	4.20
	60	3.69±0.30	2.64	4.20

Table 5. Mean Radii of Gyration of Mesopores of Various Wood Charcoals

Wood Species	Retention Time s	R_g Å	$q_{minimum} \times 10^2$ Å^{-1}	$q_{maximum} \times 10^2$ Å^{-1}
Siberian Elm	35	76.8±3.5	1.68	2.10
	60	82.3±4.9	1.62	2.00
Black Locust	35	67.6±4.1	1.60	2.00
	60	79.8±5.6	1.51	1.97
Silver Maple	35	49.1±3.2	1.74	2.16
	60	54.7±4.5	1.68	2.23

power of the calculated value of R_g for the sample; a quantity proportional to the total number of scattering entities (Kalliat et al., 1984), that is, the micropores. It is apparent from the plots that the total number of micropores present in each species decreases as τ is increased. Thus, the phenomena of the individual growth of pores together with the possible merger of adjacent pores, both substantiated by the observations for the micropores, can be expected to occur also in the *mesopores* of each sample. Although there is lack of evidence from other independent methods, it can be speculated that such an expansion-opening process does take place in the mesopores. This results in a smoothening of the interfaces, and consequently, in a reduction in the value of d_{SF}.

The problem of evaluating R_g of the mesopores from the scattering data for each sample of charcoal is a complex one. In order to highlight this aspect, the region in the vicinity of the observed shoulder has been investigated, and the Guinier plot for Siberian Elm is shown in Figure 12. At first glance, it may not be evident that the Guinier analysis for the mesopores would generate erroneous values for R_g. Upon careful examination, however, it can be discerned that the intensity in this region is the sum of the intensities scattered by the mesopores *and* macropores. This can be easily demonstrated by utilizing appropriate fitting functions for the scattering from these two pores (Kalliat et al., 1981), wherein the non-negligible scattering contribution of the macropores around the shoulder region is observed. Furthermore, it can be shown that the two intensities overlap to a considerable extent when the difference between the average dimensions of the mesopores and macropores is not appreciable. Thus, R_g of the mesopores computed from the Guinier plot of the *total* scattered intensity under these circumstance is highly inaccurate; the correct value can be obtained from the intensity curve for the mesopores only.

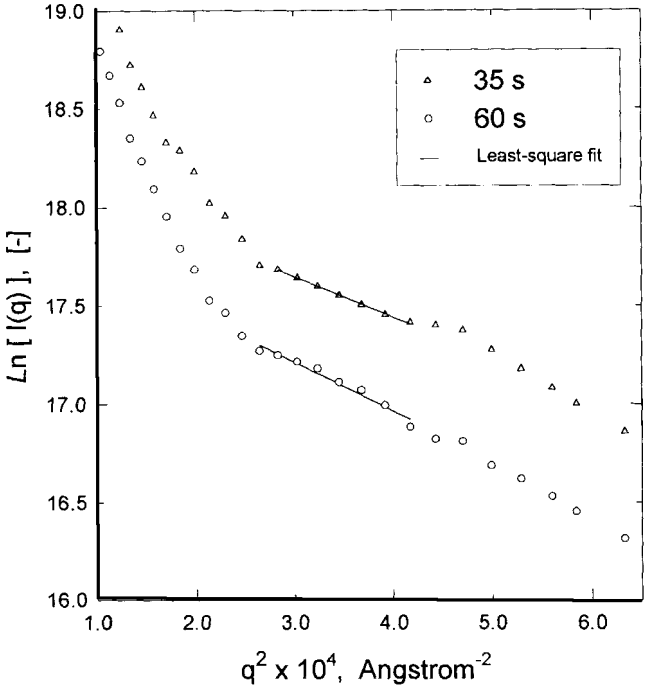

Figure 12. Guinier plot for estimating the mean radii of gyration of mesopores of Siberian Elm at various retention times.

An alternative approach to the Guinier analysis is to perform a weighted least-square fit of the scattering data through a function of the form

$$I(q) = Aq^{-\alpha} + B/(q^2 + b^2)^2$$

and extract R_g of the mesopores from the parameter, b (Schmidt et al., 1995). Nevertheless, the errors associated with the fits for all the samples of charcoals have resulted in relatively large uncertainties in the values of R_g; consequently, a meaningful comparison of R_g's could not be carried out.

Despite these shortcomings, it cannot be ruled out that the mesopores of all charcoals exhibit trends in the variation of R_g with τ, consistent with those observed for the micropores. It will be interesting to compare the results of SAXS and SEM analyses on the behavior of the pores with increased τ's, with those from other independent techniques such as gas adsorption and mercury porosimetry. We anticipate performing future investigations in this direction.

Concluding Remarks

The surface fractal dimensions, d_{SF}'s, of wood species, namely, Siberian Elm, Black Locust, and Silver Maple, and their terminal charcoals at various retention times of τ's, have been determined through the small-angle X-ray scattering technique that has the capability of characterizing porous structures with dimensions ranging from 5 to 4,000 Å. The values of d_{SF} are approximately 2.05±0.10 for all the original wood species prior to pyrolysis; the corresponding values for the charcoals lie within the range from 2.4 to 2.8. An unforeseen propensity in the variation of d_{SF} with τ has also been discerned for all the wood charcoals. These results obtained during the pyrolysis of a naturally occurring product may prove to be beneficial for investigating the influence of fractal surfaces on the rates of heterogeneous gas–solid reactions.

Acknowledgment

The authors would like to thank Dr. Sajan Thomas for his assistance in obtaining the X-ray scattering data. The authors would also like to thank one of the reviewers for his constructive criticisms and recommendations. This is contribution #90-323-J, Department of Chemical Engineering, Kansas Agricultural Experiment Station, Kansas State University, Manhattan, KS 66506.

Notation

$I(0)$ = extrapolated value of the scattered intensity for q equal to zero
I_e = intensity scattered by a single electron
Γ = gamma function of Eq. 8
μ_m = mass absorption coefficient of a sample, m^2/kg
ρ = specific gravity of a sample, kg/m^3
τ = retention time, s

Literature Cited

Adler, P. M., "Flow in Porous Media," *The Fractal Approach to Heterogeneous Chemistry: Surfaces, Colloids, and Polymers*, D. Avnir, ed., Wiley, Chichester, England, p. 345 (1989).

Adler, P. M., *Porous Media: Geometry and Transports*, Butterworth-Heinemann, Boston, p. 47 (1992).

Anderegg, J. W., Beeman, W. W., Shulman, S., and P. Kaesberg, "An Investigation of the Size, Shape, and Hydration of Serum Albumin by Small-Angle X-ray Scattering," *J. Amer. Chem. Soc.*, **77**, 2929 (1955).

Avnir, D., and D. Farin, "A Discussion of Some Aspects of Surface Fractality and of its Determination," *New J. Chem.*, **16**, 439 (1992).

Avnir, D., D. Farin, and P. Pfeifer, "Chemistry in Noninteger Dimensions between Two and Three. II. Fractal Surfaces of Adsorbents," *J. Chem. Phys.*, **79**, 3566 (1983).

Avnir, D., D. Farin, and P. Pfeifer, "Molecular Fractal Surfaces," *Nature*, **308**, 261 (1984).

Bale, H. D., M. L. Carlson, M. Kalliat, C. Y. Kwak, and P. W. Schmidt, "Small-Angle X-ray Scattering of the Submicroscopic Porosity of Some Low-Rank Coals," *The Chemistry of Low-Rank Coals*, H. H. Schobert, ed., ACS Symp. Ser. 264, Washington, DC, p. 79 (1984).

Bale, H. D., and P. W. Schmidt, "Small-Angle X-Ray-Scattering Investigation of Submicroscopic Porosity with Fractal Properties," *Phys. Rev. Lett.*, **53**, 596 (1984).

Beeman, W. W., *Small-Angle X-ray Scattering*, H. H. Brumberger, ed., Gordon & Breach, New York, p. 198 (1967).

Bevington, P. R., *Data Reduction and Error Analysis for the Physical Sciences*, McGraw-Hill, New York, p. 106 (1969).

Bhatia, S. K., and D. D. Perlmutter, "A Random Pore Model for Fluid-Solid Reactions: I: Isothermal, Kinetic Control," *AIChE J.*, **26**, 379 (1980).

Bhatia, S. K., and D. D. Perlmutter, "The Effect of Pore Structure on Fluid-Solid Reactions: Application to the SO_2-Lime Reaction," *AIChE J.*, **27**, 226 (1981).

Boateng, A. A., L. T. Fan, W. P. Walawender, and C. S. Chee, "Morphological Development of Rice-Hull-Derived Charcoal in a Fluidized-Bed Reactor," *Fuel*, **70**, 995 (1991).

Boateng, A. A., L. T. Fan, W. P. Walawender, C. S. Chee, and S. M. Chern, "Kinetics of Rice Hull Char Burnout in a Bench-Scale Fluidized-Bed Reactor," *Chem. Eng. Commun.*, **113**, 117 (1992).

Compton, A. H., and S. K. Allison, *X-Rays in Theory and Experiment*, 2nd ed., Van Nostrand, New York, pp. 9, 802 (1935).

Coppens, M. O., and G. F. Froment, "Diffusion and Reaction in a Fractal Catalyst Pore: I. Geometrical Aspects," *Chem. Eng. Sci.*, **50**, 1013 (1995a).

Coppens, M. O., and G. F. Froment, "Diffusion and Reaction in a Fractal Catalyst Pore: II. Diffusion and First-Order Reaction," *Chem. Eng. Sci.*, **50**, 1027 (1995b).

Cutter, B. E., E. A. McGinnes, and P. W. Schmidt, "X-Ray Scattering and X-Ray Diffraction Techniques in Studies of Gamma-Irradiated Wood," *Wood & Fiber*, **11**, 228 (1980).

Dullien, F. A. L., *Porous Media: Fluid Transport and Pore Structure*, 2nd ed., Academic Press, San Deigo, p. 64 (1992).

Fan, L. T., D. Neogi, and M. Yashima, *An Elementary Introduction to Spatial and Temporal Fractals*,, Springer-Verlag, Berlin, p. 30, 116 (1991).

Feder, J., *Fractals*, Plenum Press, New York, p. 213 (1988).

Fripiat, J. J., L. Gatineau, and H. Van Damme, "Multilayer Physical Adsorption on Fractal Surfaces," *Langmuir*, **2**, 562 (1986).

Gates, C. G., *Catalytic Chemistry*, Wiley, New York, pp. 131, 225 (1992).

Gavalas, G. R., "A Random Capillary Model with Application to Char Gasification of Chemically Controlled Rates," *AIChE J.*, **26**, 577 (1980).

Glatter, O., and O. Kratky, *Small-Angle X-ray Scattering*, Academic Press, New York, pp. 126, 167 (1982).

Guinier, A., G. Fournet, C. B. Walker, and K. L. Yudowitch, *Small-Angle Scattering of X-Rays*, Wiley, New York, pp. 3, 7, 24, 78, 80, (1955).

Gutfraind, R., and M. Sheintuch, "Scaling Approach to Study Diffusion and Reaction Processes on Fractal Catalysts," *Chem. Eng. Sci.*, **47**, 4425 (1992).

Gutfraind, R., M. Sheintuch, and D. Avnir, "Fractal and Multifractal Analysis of the Sensitivity of Catalytic Reactions to Catalyst Structure," *J. Chem. Phys.*, **95**, 6100 (1991).

Hall, P. G., and R. T. Williams, "An Investigation of Surface Area and Porosity in Solids by Small-Angle Neutron Scattering (SANS)," *J. Coll. Interf. Sci.*, **104**, 151 (1985).

Hendricks, R. W., and P. W. Schmidt, "Calculation of the Weighting Functions for Collimation Corrections in Small-Angle X-Ray Scattering," *Acta Phys. Austriaca*, **26**, 97 (1967).

Hohr, A., H. Neumann, P. W. Schmidt, P. Pfeifer, and D. Avnir, "Fractal Surface and Cluster Structure of Controlled Pore Glasses and Vycor Porous Glasses as Revealed by Small-Angle X-Ray and Neutron Scattering," *Phys. Rev. B*, **38**, 1462 (1988).

Kalliat, M., D. H. Finseth, and P. W. Schmidt, "Observation of Colloidal Growth in Coal Liquids," *Fuel*, **63**, 1178 (1984).

Kalliat, M., C. Y. Kwak, and P. W. Schmidt, "Small-Angle X-ray Investigation of the Porosity of Coals," *New Approaches in Coal Chemistry*, B. D. Blaustein, B. C. Bockrath, and S. Freidman, eds., ACS Symp. Ser. 169, Washington, DC, p. 3 (1981).

Lin, J. S., C. R. Von Bastian, and P. W. Schmidt, "A Modified Method for Slit-Length Collimation Corrections in Small-Angle X-Ray Scattering," *J. Appl. Cryst.*, **7**, 439 (1974).

Mandelbrot, B. B., *The Fractal Geometry of Nature*, Freeman, San Francisco, p. 25 (1982).

Margerison, D., *Comprehensive Chemical Kinetics*, Elsevier, Amsterdam, p. 404 (1969).

Pape, H., L. Riepe, and J. R. Schopper, "The Role of Fractal Quantities, as Specific Surface and Tortuosities, for Physical Properties of Porous Media," *Part. Charact.*, **1**, 66 (1984).

Pfeifer, P., and D. Avnir, "Chemistry in Non-Integer Dimensions between Two and Three: I. Fractal Theory of Heterogeneous Surfaces," *J. Chem. Phys.*, **79**, 3558 (1983).

Pfeifer, P., D. Avnir, and D. Farin, "Ideally Irregular Surfaces of Dimension Greater than Two, in Theory and Practice," *Surf. Sci.*, **126**, 569 (1983).

Pfeifer, P., and P. W. Schmidt, "Porod Scattering from Fractal Surfaces," *Phys. Rev. Lett.*, **60**, 1345 (1988).

Pfeifer, P., Y. J. Wu, M. W. Cole, and J. Krim, "Multilayer Adsorption on a Fractally Rough Surface," *Phys. Rev. Lett.*, **62**, 1997 (1989).

Pines, D., and D. Hubbert, "Time-Resolved Fluorescence Depolarization Measurements in Mesoporous Silicas. The Fractal Approach," *J. Phys. Chem.*, **91**, 6569 (1987).

Pines, D., D. Hubbert, and D. Avnir, "The Fractal Nature of the Surfaces of Porous Silicas as Revealed in Electronic Energy Transfer Between Adsorbates: Comparison of Three Donor/Acceptor Pairs," *J. Chem. Phys.*, **89**, 1177 (1988).

Porod, G., *Kolloid Z.*, **124**, 93 (1951).

Rojanski, D., D. Huppert, H. D. Bale, X. Dacai, P. W. Schmidt, D. Farin, A. Seri-Levy, and D. Avnir, "Integrated Fractal Analysis of Silica: Adsorption, Electronic Energy Transfer, and Small-Angle X-ray Scattering," *Phys. Rev. Lett.*, **56**, 2505 (1986).

Satterfield, C. N., *Mass Transfer in Heterogeneous Catalysis*, M. I. T. Press, Cambridge, MA, p. 138 (1970).

Satterfield, C. N., and T. K. Sherwood, *The Role of Diffusion in Catalysis*, Addison-Wesley, London, p. 56 (1963).

Schmidt, P. W., "Use of Scattering to Determine the Fractal Dimension," *The Fractal Approach to Heterogeneous Chemistry: Surfaces, Colloids, and Polymers*, D. Avnir, ed., Wiley, Chichester, England, p. 67 (1989).

Schmidt, P. W., "Small-Angle Scattering Studies of Disordered, Porous and Fractal Systems," *J. Appl. Cryst.*, **24**, 414 (1991).

Schmidt, P. W., "Small-Angle Scattering Studies of Solids with Disorder on Length Scales from about 5 to 2000 A," *Proc. Conf. on Applied Crystallography*, Cieszyn, Poland, August 22–26 (1994).

Schmidt, P. W., D. Avnir, H. B. Neumann, A. Hoehr, M. Steiner, D.

Levy, V. R. Kaufman, J. Lin, Y. M. Kapoor, and J. S. Lin, "Small-Angle X-Ray Scattering Study of Two-Length Scale Structure in some Silica Xerogels," unpublished research, p. 1 (1995).
Schmidt, P. W., A. Hoehr, H. B. Neumann, H. Kaiser, D. Avnir, and J. S. Lin, "Small-Angle X-Ray Scattering Study of the Fractal Morphology of Porous Silicas," *J. Chem. Phys.*, **90**, 5016 (1989).
Seri-Levy, A., and D. Avnir, "Fractal Analysis of Surface Geometry Effects on Catalytic Reactions," *Surf. Sci.*, **248**, 258 (1991).
Setek, M., I. K. Snook, and H. K. Wagenfeld, "Determination of the Microstructure of Wet and Dry Brown Coal by Small-Angle X-Ray Scattering," *The Chemistry of Low-Rank Coals*, H. H. Schobert, ed., ACS Symp. Ser. 264, Washington, DC, p. 95 (1984).
Sheintuch, M., and S. Brandon, "Deterministic Approaches to Problems of Diffusion, Reaction, and Adsorption in a Fractal Porous Catalyst," *Chem. Eng. Sci.*, **44**, 69 (1989).
Su, J. L., and D. D. Perlmutter, "Effect of Pore Structure on Char Oxidation Kinetics," *AIChE J.*, **31**, 973 (1985).
Wong, P. Z., and A. J. Bray, "Small-Angle Scattering by Rough and Fractal Surfaces," *J. Appl. Cryst.*, **21**, 786 (1988a).
Wong, P. Z., and A. J. Bray, "Porod Scattering from Fractal Surfaces," *Phys. Rev. Lett.*, **60**, 1344 (1988b).

Appendix: Corrections to $I(q)$ for Differing Thickness of Samples

The measured value of the transmission, T, for each sample is related to M/A_0 through the following equation (Compton and Allison, 1935):

$$T = \exp(-\mu_m M/A_0). \tag{A1}$$

Taking the natural logarithm of both sides of Eq. A1 and rearranging the resulting terms yields

$$\ln(1/T) = \mu_m M/A_0. \tag{A2}$$

The total volume of each sample irradiated, V, can be expressed as

$$V = (M/A_0) * (A_0/\rho). \tag{A3}$$

The normalized scattered intensity for each sample is, therefore, obtained by dividing the measured values of $I(q)$ by the total volume, given by Eq. A3,

$$I(q)/V = I(q)/[(M/A_0) * (A_0/\rho)]$$

or

$$I(q)/V = \mu_m I(q)/[(\mu_m M/A_0) * (A_0/\rho)]. \tag{A4}$$

Combining Eqs. A2 and A4 yields

$$I(q)/V = \mu_m I(q)/[\ln(1/T) * (A_o/\rho)]$$

or alternatively,

$$I(q)/V = [\mu_m \rho/\ln(1/T)][I(q)/A_0]. \tag{A6}$$

Since A_0 is the same for all samples, the correction factor to account for possible differences in the thickness of each sample is $\mu_m \rho/\ln(1/T)$, as given in the subsection, SAXS, in the section titled "Experimental."

Manuscript received Feb. 3, 1995, and revision received Oct. 23, 1995.